(Preprint) AAS 19-455

CONNECTING RESONANT TRAJECTORIES TO A EUROPA CAPTURE THROUGH LISSAJOUS STAGING ORBITS

Sonia Hernandez*, Ricardo L. Restrepo†, and Rodney L. Anderson‡

The current interest in studying the surface of Europa in search of biosignatures demands efficient strategies in mission design to reach this distant world. An affordable strategy is to use a low energy moon tour, which has natural access to the moon via the L_2 gateway. Staging around this libration point allows to decouple the approaching moon tour and the landing trajectory, which enables the option of designing each phase separately. Furthermore, a staging step frees the landing time from the capture phase, adding an additional degree of freedom. Lissajous orbits are the dynamical structures used for these staging orbits. In this paper, the possible ballistic connections between the resonances from the moon tour and Lissajous orbits are studied, including the different geometries that allow for time phasing control.

INTRODUCTION

Scientists are eager to explore Europa, the icy moon of Jupiter, due its potential to harbor life. Taking in situ measurements is key in the search of biosignatures, for which a probe that lands of the surface is needed. A low-energy trajectory can provide a fuel efficient mechanism to approach Europa (typical two-body patched conic design would be too expensive for this type of mission). To get captured at this moon, a general strategy which has been proposed in the past for orbiter missions is to use a moon tour after Jupiter insertion to gradually reduce the two-body energy of the spacecraft. The moon tour involves using three-body gravity assists of Ganymede and Europa (and in some cases Callisto), in a resonant hopping sequence. Once close enough to Europa, the L_2 gateway is the natural access to a capture orbit. Libration point orbits and their manifolds provide the capture mechanisms and are also useful as staging orbits for phasing purposes. To land on the surface, an additional phase is required that connects the capture phase to a target landing location.

A lander-type mission can have a lot of mission constraints, including lighting conditions at the time of landing, staging locations to decouple the approach to Europa, etc. These constraints can make this quite a complex trajectory to design. For this reason it is preferable to divide the trajectory design after Jupiter insertion into three separate steps, breaking the highly coupled problem into independent phases: 1) the moon tour, 2) a low-energy capture in the vicinity of Europa and a

*Mission Design and Navigation Engineer, Jet Propulsion Laboratory, California Institute of Technology, 4800 Oak Grove Drive, Pasadena, CA 91109. Corresponding Author: Sonia Hernandez; *Tel*: (818) 354-0418; *E-mail address*: Sonia.Hernandez-Doran@jpl.nasa.gov.

†Postdoc fellow, Jet Propulsion Laboratory, California Institute of Technology, 4800 Oak Grove Drive, Pasadena, CA 91109. *E-mail address*: ricardo.rpo@utexas.edu.

‡Mission Design Engineer, Jet Propulsion Laboratory, California Institute of Technology, 4800 Oak Grove Drive, Pasadena, CA 91109. *E-mail address*: rodney.anderson@jpl.nasa.gov.

phasing stage, and 3) the landing.[1] The work presented here focuses on the second phase of the problem.

The dynamical structures used to construct the framework of the capture and phasing are libration point orbits and their invariant manifolds. The invariant manifolds of unstable periodic orbits at the L_1 and L_2 libration points have been shown to be key to understanding the approach problem. Previous work explored this relationship for the Moon[2–5] and for Europa.[6,7] Of the libration point orbits, the most widely studied dynamical structures are Lyapunov[8] and halo[9] orbits. Lyapunov orbits are the most basic libration point orbits, as they are planar, periodic, and centered around L_1 and L_2. Only one family exists associated to each libration point,[8] and within the family, each obit exhibits a different energy (or Jacobi constant). At a specific energy level, two families of out-of-plane periodic orbits emerge from a specific Lyapunov: southern and northern halo orbits. A more complex dynamical structure, called Lissajous orbits, is formed by a combination of an in-plane and out-of-plane frequency. While Lyapunov and halo orbits are periodic, Lissajous are quasi-periodic orbits that live in the surface of a torus. Also, while only one orbit per energy level exists for Lyapunov and halos, the in-plane and out-of-plane amplitude of the Lissajous can be combined to create multiple sets of continuous families at a fixed energy level. While we explore Lyapunov and halo orbits as options to get captured at Europa, we focus our efforts on Lissajous orbits because they allow for a wider set of arrival capture configurations.

Mission Design from a Resonance to Capture/Landing Trajectory

Figure 1 shows a schematic of the second stage of the mission, i.e., the low-energy Europa capture phase, departing from a resonant orbit, arriving at a staging orbit around L_2, and ending with two different landing scenarios. In this example, the resonant hopping moon tour ends in a 5:6 resonant orbit*, from where a Δv-free low-energy capture is possible. A loosely captured orbit around L_2 follows, giving the option of several revolutions around the libration point for phasing purposes. Following the loose capture, two landing options are represented: a) a free, direct landing trajectory that departs from the libration orbit, following the natural flow of its unstable manifold,[1] and b) a capture into a stable, two-body orbit around Europa, enabled by an insertion orbit maneuver. In the latter scenario, the spacecraft can do reconnaissance of Europa before performing the maneuver to land. If the lander is accompanied by a carrier spacecraft, this scenario also allows for the carrier to stay in the stable orbit and act as a relay to the lander.

A systematic strategy for the trajectory design of the second stage of the mission is adopted, where stable and unstable manifolds of libration point orbits are computed to connect the libration staging orbit with the low-energy resonant capture (propagated backward in time) and the landing/stable capture (propagated forward in time). The goal of the paper is to determine which resonances and range of energies freely connect with these libration point orbits by propagating their invariant manifolds backward in time. This strategy also enables the characterization of different geometry arrival conditions at the libration point orbit, which in turns allows for a timing leverage, necessary to land on the surface of Europa at a desired local solar time. In Reference 1, Restrepo et al. studied Europa landing surface coverage provided by the unstable invariant manifolds of Lissajous orbits around L_2 propagated forward in time (Figure 1(a)). They found that by using a direct landing approach, almost full coverage of the surface can be achieved. Even though this method provides a Δv-free approach, it could be a challenge to navigate the spacecraft to the landing site due to the

*A 5:6 resonant orbit is defined in this paper as 6 revolutions of the spacecraft around Jupiter for every 5 revolutions of Europa, in an inertial frame.

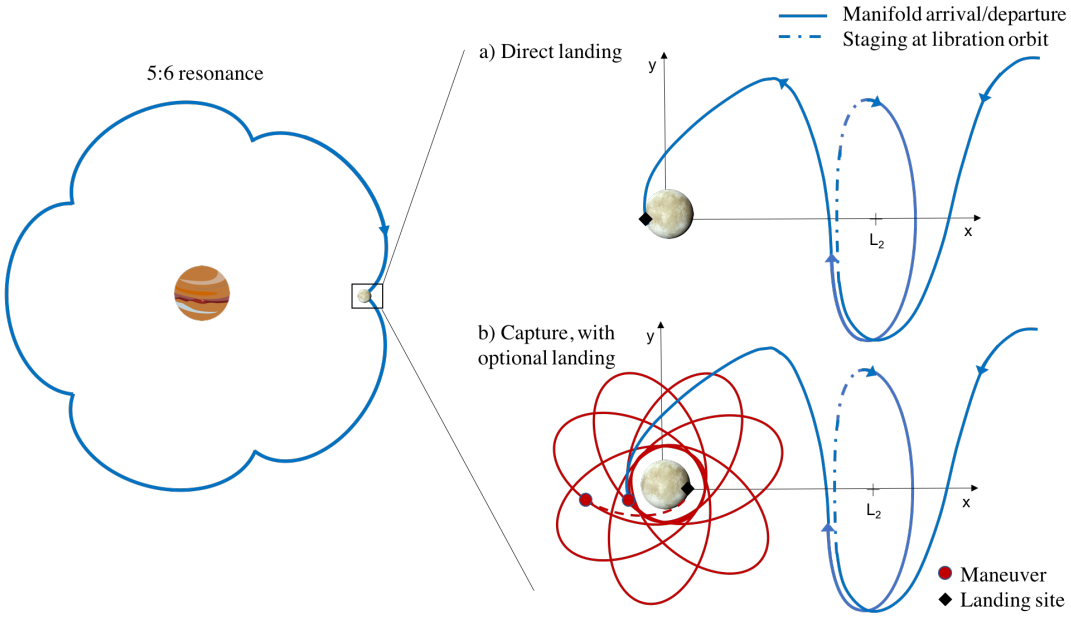

Figure 1. Using libration point orbits to connect the last resonant orbit of a moon tour with a landing/capture trajectory at Europa.

instability of the manifold and the short amount of time allowed to accurately determine Europa's orbit state. For this reason, a scenario where a two-body capture is performed before landing might desired (Figure 1(b)), where there is ample time to reduce Europa's state uncertainty, and orbit trim maneuvers can ensure accurate landing. This last scenario will be documented in future work.

The paper is organized as follows. The first section focuses on Lyapunov and halo orbits as loose-capture orbit options, where the possible reachable resonances from these periodic orbits are investigated. Lissajous orbits are the next type of libration point orbit studied and the main focus of the paper. A database of Lissajous orbits is generated with details presented in the following section. The next section investigates the possible reachable resonances from Lissajous orbits. Timing and geometry arrival scenarios are investigated in the following section. The last section concludes the paper and discusses avenues of future work.

REACHABLE RESONANCES FROM LYAPUNOV AND HALO ORBITS

To begin the study of which resonances are available and at what energy levels, Lyapunov and halo orbits are used as libration point orbits at L_2. The general strategy to approach Europa is through a sequence of high altitude three-body flybys to reduce the spacecraft's two-body energy with respect to Jupiter. For this sequence of flybys to be possible, they have to occur through a set of resonant sequences in order to guarantee the periodicity of the encounter of the spacecraft with Europa. Therefore, the leg of the trajectory that connects with the libration point (forward in time) must be a resonant trajectory. This leg is selected from the set of trajectories that compose the stable manifolds that arrive at the libration point orbit, and they are computed backward in time.

Computation of Invariant Manifolds of Periodic Orbits The computation of the stable and unstable invariant manifolds of a periodic orbit are obtained by perturbing each point of the orbit along

a specific stable and an unstable direction. This procedure is described in detail in Ref. 10, 11. The direction of the perturbation is given by the eigenvectors of the monodromy matrix ($\mathbf{\Phi}(T, t_0)$), which is the state transition matrix (STM) evaluated after one orbit period (T). The eigenvalues of the monodromy matrix of an unstable periodic orbit will in general contain four eigenvalues of unit magnitude and two that form a complementary pair of asymptotically stable ($\lambda < 1$) and unstable ($\lambda > 1$) values. The corresponding eigenvectors associated with the unit magnitude eigenvalues are a complex conjugate pair and a repeated real pair. The additional two eigenvalues are associated with two fully real vectors, which are the ones used to excite the stable and unstable motion around the periodic orbit. The eigenvector $\mathbf{V}_u(t_0)$ with real eigenvalue greater than 1 provides the unstable direction; the eigenvector $\mathbf{V}_s(t_0)$ with reciprocal eigenvalue less than 1 provides the stable direction. To compute the stable and unstable directions at any point over the orbit, the STM is used as a linear mapping. For example, the unstable directions along the orbit are given by:

$$\mathbf{V}_u(\tau) = \mathbf{\Phi}(\tau, t_0)\mathbf{V}_u(t_0) \tag{1}$$

where τ is a normalized variable ($\tau = 0 \rightarrow 1$) introduced to represent the time discretization along one period of the orbit, such that $t_i = t_0 + \tau T$. The manifold trajectories are obtained by propagating the perturbed states

$$\mathbf{X}_u(\tau) = \mathbf{X}(\tau) \pm \epsilon \hat{\mathbf{V}}_u(\tau) \tag{2}$$

where $\hat{\mathbf{V}}_u(\tau) = \mathbf{V}_u(\tau)/||\mathbf{V}_u(\tau)||$, and ϵ is a small parameter ($\epsilon << 1$) that represents the magnitude of the perturbation.

Halo and Lyapunov Orbit Comparison

Lyapunov and halo orbits are computed for a range of Jacobi constants from 3.00318 (low energy) to 3.001 (high energy), and are shown in Figure 2. The halo and Lyapunov orbit stable manifolds propagated backward in time are projected into the xy-plane and plotted in Figure 3 for the two bounding set of energies. It can be seen that the stable manifolds of the halo and Lyapunov orbits are similar near the upper end of the Jacobi constant range at C = 3.00318. This result is because the halo orbit at this energy has just bifurcated from the planar Lyapunov orbit family, and it does not at this point have a very large z component. As the Jacobi constant decreases and the energy correspondingly increases, the differences in the stable manifold trajectories become more apparent. At this point, the halo orbit family has a significant component that is out of the plane, and it is easier to explore the difference by comparing several other parameters related to the period and orbital elements.

One of the primary considerations in the approach problem for Europa is connecting the approach trajectory to the last exterior resonance of the endgame. This connection is typically analyzed initially by considering either the period or the semi-major axis as these quantities provide a good osculating two-body approximation to the resonance and the corresponding resonant orbit in the Circular Restricted Three-Body Problem. These quantities are plotted as a function of several different parameters for several selected Jacobi constants across the desired range in Figure 4. As would be expected from the projection plots in xy the resulting characteristics of the stable manifolds are most similar near the upper range of the Jacobi constants where the orbits themselves are similar. For lower Jacobi constants, it can be observed that the Lyapunov orbits have the larger

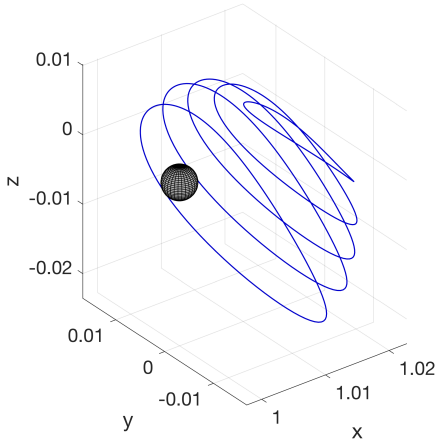

(a) Halo orbits for a range of energies

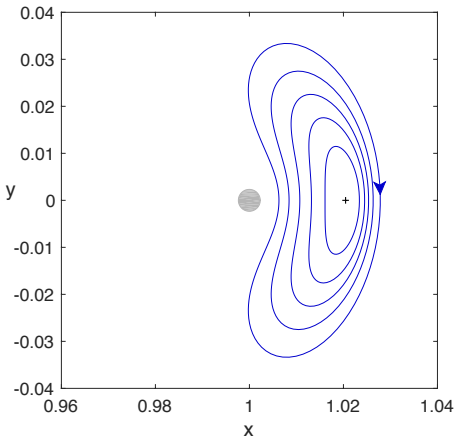

(b) Lyapunov orbits for a range of energies

Figure 2. The Lyapunov and halo orbit families.

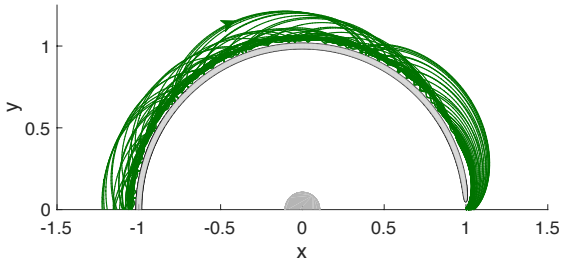

(a) Halo Orbit, C = 3.0010

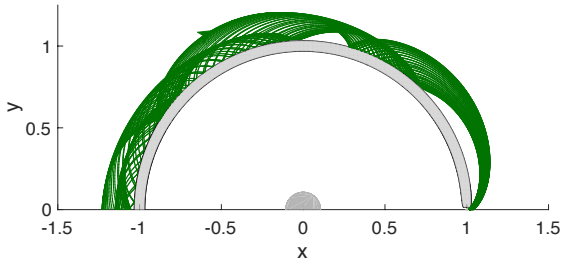

(b) Halo Orbit, C = 3.00318

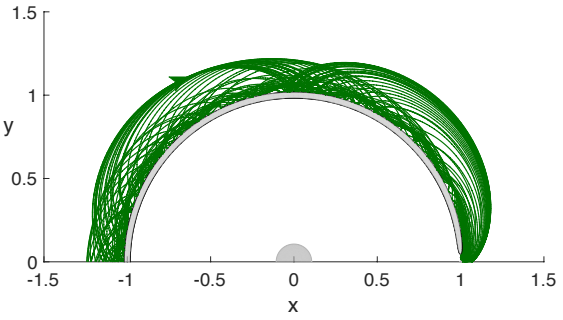

(c) Lyapunov Orbit, C = 3.0010

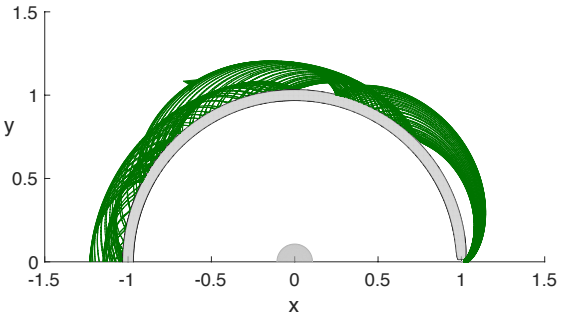

(d) Lyapunov Orbit, C = 3.00318

Figure 3. The Lyapunov and halo orbit stable manifolds plotted for a Jacobi constants $J = 3.0018$.

range of period and semi-major axis. This is consistent with what was seen in Anderson and Lo[7] where the Lyapunov orbits provided a general bounds on the resonance.

This difference in the range of the semi-major axis or period may perhaps be seen even more clearly by the direct comparison in Figure 5. Noting the differences in the scales, it can be seen that the semi-major axis range consistently grows for the Lyapunov orbits as the Jacobi constants decrease. The trend for the halo orbits is different, and the semi-major axis range remains fairly

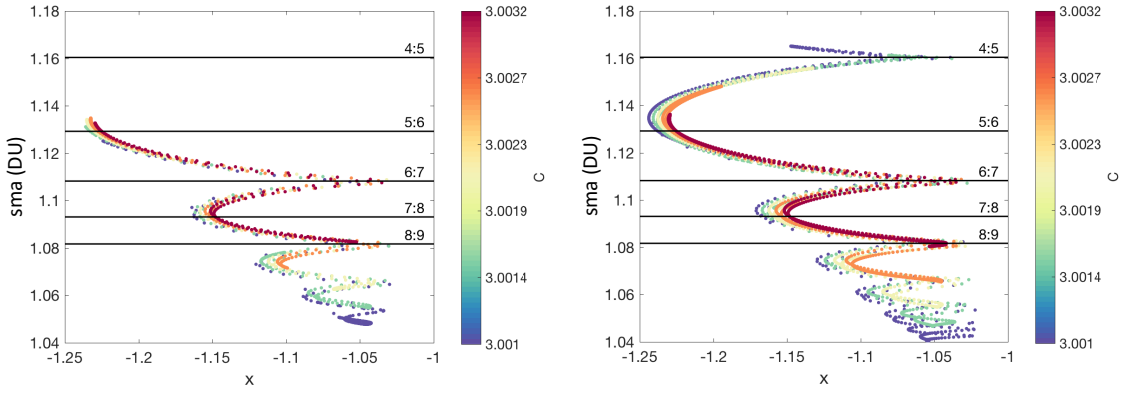

(a) Halo Orbit (b) Lyapunov Orbit

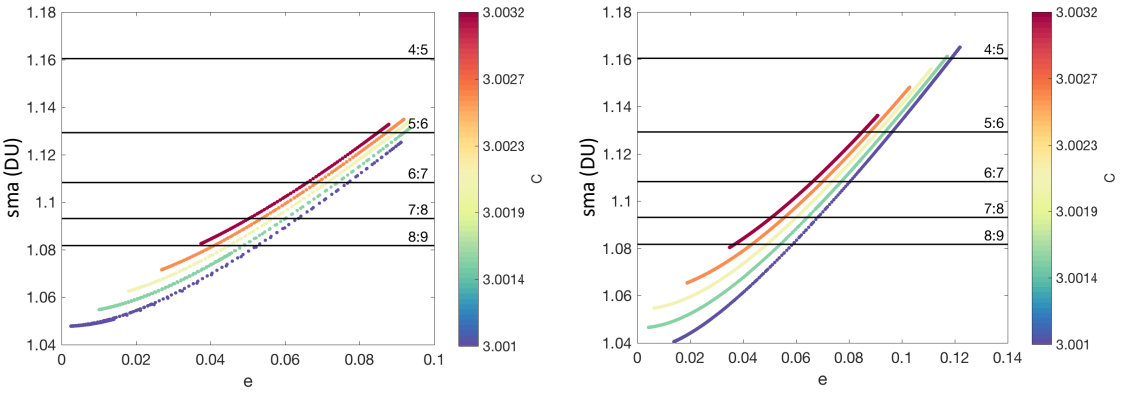

(c) Halo Orbit (d) Lyapunov Orbit

Figure 4. The semi-major axis and period of the halo and Lyapunov orbit stable manifold trajectories at the surface of section plotted as a function of various parameters.

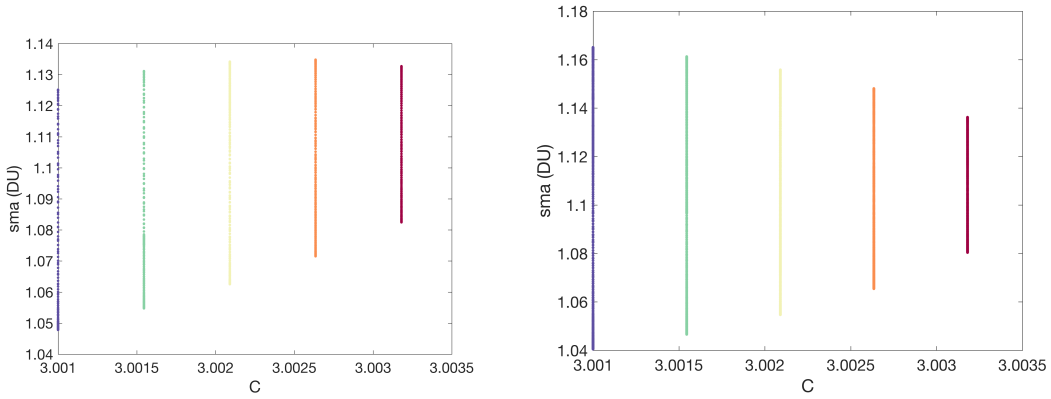

(a) Halo Orbit (b) Lyapunov Orbit

Figure 5. Comparison of the range of semimajor axis for the halo orbit and Lyapunov stable manifolds for various Jacobi constants.

constant for lower Jacobi constants after some initial growth when the Jacobi constant decreases from 3.0032. Again, this may be partly explained by the fact that some of the growth of the halo orbit is now in the z direction and this is likely limiting some of the growth in the stable manifold semi-major axis that would be expected.

One other parameter that is important in the trajectory design is the location on the orbit (τ) that the stable manifold approaches. This quantity is plotted for all of the computed orbits in Figure 6. For low energy Lyapunov and halo orbits, the behavior plotted is perfectly sinusoidal, repeating after one orbit period. However, as the energy increases (lower Jacobi constant), this behavior begins to break down due to the instability of the periodic orbits. For both the halo and Lyapunov orbits orbits, depending on where you depart the orbit, you may be able to reach different resonances. This result is key when working on the last resonant orbit of the moon tour.

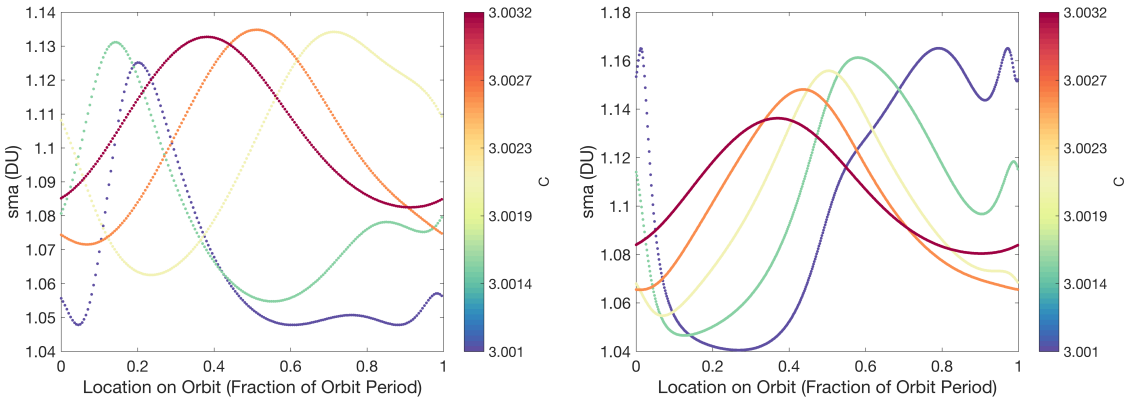

(a) Halo Orbit (b) Lyapunov Orbit

Figure 6. Location on each orbit that the stable manifold approaches for various semimajor axis values for a linear offset of 1.0×10^{-6}.

GENERATING A DATABASE OF LISSAJOUS ORBITS

Lissajous orbits are quasi-periodic structures associated to each of the collinear libration points of the circular restricted three-body problem (i.e., L_1, L_2 and L_3). These three-dimensional structures are bounded trajectories constrained to the surface of a two-dimensional object, known as an invariant torus. Computing the manifolds of an invariant torus can be complicated and computationally expensive. To simplify the process, individual revolutions (revs) of Lissajous trajectories are considered as approximate periodic orbits. For each Lissajous rev, approximate stable and unstable manifolds are computed by using standard techniques to compute the invariant manifolds of periodic orbits.[10–12] The approximate stable invariant manifolds, propagated backward in time, are used to connect with the last resonance of the moon tour. Each Lissajous is used as a temporary station or staging orbit to satisfy the phasing requirement for a capture/landing trajectory. The generation of Lissajous orbits and their approximate invariant manifolds have been described in detail in Reference 1 and are briefly summarized here for completeness.

Lissajous orbits are symmetric with respect to the x-y plane and the x-z plane, and can be characterized by an in-plane amplitude A_y and an out-of-plane amplitude A_z. Lissajous orbits can be periodic for exact resonances between the in-plane and out-of-plane frequencies, but in general they

are not, and in this case their trajectories can exist at any point in the surface of a two-dimensional torus. Two initial phases ϕ and ψ can be used to define a particular trajectory over the torus, where ψ is a phase associated with the out-of-plane motion and ϕ to the in-plane phase.[13] Figure 7 shows three different views of a Lissajous orbit propagated for 27 revs, centered around L_2 in the Jupiter-Europa system, with associated amplitudes $A_y = 4500$ km and A_z =4500 km. The initial conditions of the trajectory are such that it begins in the x-y plane at $y = 0$, that is, $\psi = 0°$ and $\phi = 0°$. The non-periodicity of the orbit is observed in the y-z view, where the in-plane phase completes approximately 360°, but not exactly.

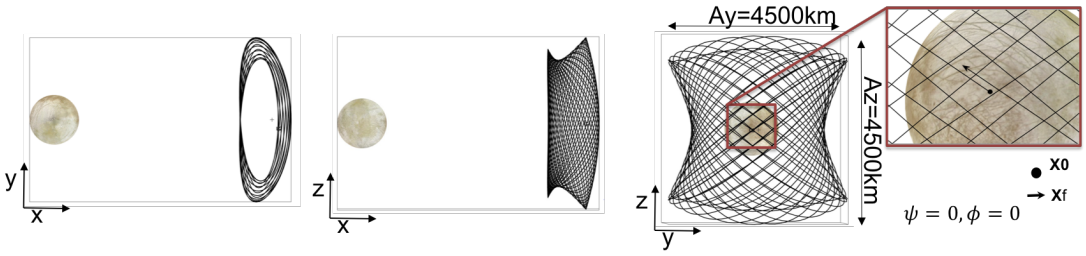

Figure 7. Lissajous orbit example around L_2.

A detailed literature review on the history of Lissajous orbits and the different schemes to compute these orbits can be found in Reference 1. The database in this paper embeds a multi-shooting technique for correcting third and fourth order analytical expansions[13] with a third-order expansion approximation.[14] The general structure of a Lissajous torus can be obtained by generating individual Lissajous revs all around its surface, as shown in Figure 8. Here, one single rev is highlighted in red. The initial conditions of this Lissajous rev start at the x-y plane ($\psi = 0$) with $\phi = 0$, and it is propagated until it completes a full out-of-plane cycle, returning to the x-y plane. To approximate the global structure of a Lissajous torus, individual revs are generated with a small in-plane phase difference ($\Delta\phi$) in their initial conditions. In Figure 8, 200 Lissajous revs are used to approximate a Lissajous torus with amplitudes A_y =4500 km and A_z =4500 km, with a phase shift of $\Delta\phi = 1.8°$ between revs. For simplicity ψ is always set to zero.

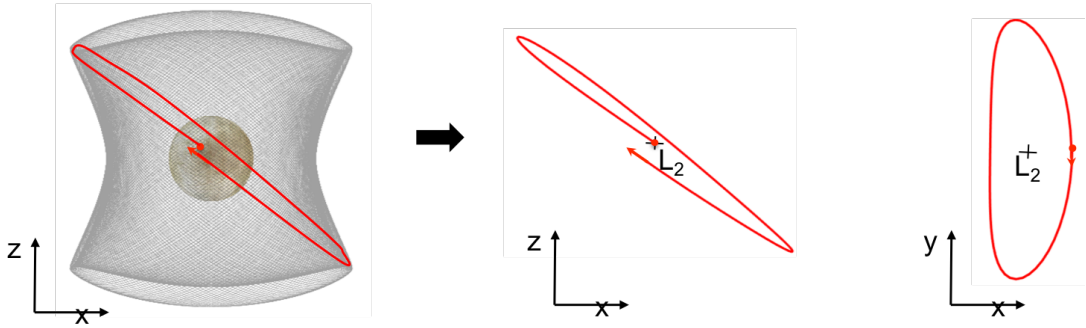

Figure 8. Lissajous torus formed by 200 individual revs. Red orbit represents a single rev, with $\psi = 0$ and $\phi = 0$.

The database of Lissajous orbits is generated by sweeping A_y from 1000 km $\leq A_y \leq$ 12000 km in 500 km intervals and A_z from 2000 km $\leq A_z \leq$ 12000 km by intervals of 100 km, for a total of 1100 Lissajous. Each Lissajous orbit is constructed with 200 individual revs (each one approximating a

periodic orbit) for a total database of 220,000 Lissajous revs.

REACHABLE RESONANCES FROM LISSAJOUS ORBITS

Each Lissajous rev, computed as described in the previous section, acts as a good approximation of a periodic orbit, which allows for the computation of approximate invariant manifolds. The invariant manifold of an entire Lissajous torus can therefore be approximated by combining the approximate invariant manifolds of each of the individual revs that approximate the torus.[1]

Approximate invariant manifolds of Lissajous orbits The intricate process of computing the invariant manifolds of an entire Lissajous torus is simplified by combining the approximate invariant manifolds of the individual Lissajous revs that conform the full torus. The STM is propagated for each rev from t_0 to T_{rev} to obtain an *approximate* monodromy matrix $\mathbf{\Phi}(T_{rev}, t_0)$. The stable and unstable invariant manifolds for each Lissajous rev are computed using the same procedure as that for periodic orbits. Note that due to the symplectic nature of the STM, the eigenvalues of this approximate monodromy matrix still come in reciprocal pairs. However, the two unity magnitude real eigenvalues found in a periodic solution no longer exist; they are now near unity, corresponding to a marginally stable and unstable eigenvector direction. The two remaining real eigenvectors, corresponding to highly stable and unstable directions, are the ones used to generate the approximate invariant manifolds of each Lissajous rev, and Eq. (2) is used to compute the perturbed states.

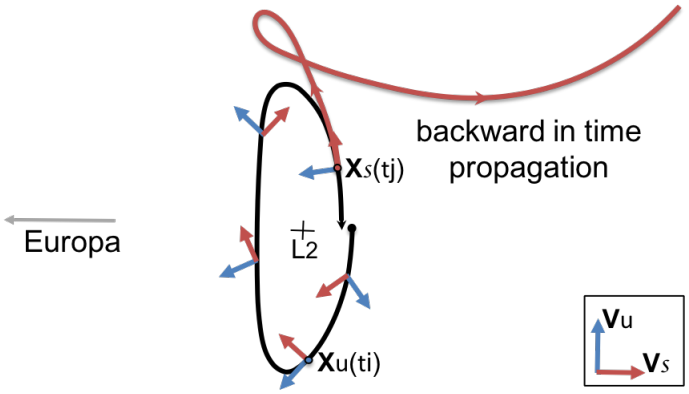

Figure 9. Schematic of stable manifold propagated backward in time for one Lissajous rev.

Figure 9 shows a schematic of a stable manifold trajectory propagated backwards in time at τ_j for one Lissajous rev. Each Lissajous rev is discretized in 100 points from t_0 to T_{rev} to generate 100 manifold trajectories per rev. Note that there are directions to perturb (positive and negative) each eigenvector. The sign of the perturbation is selected such that the stable manifolds move (backward in time) away from Europa.

Figure 10 shows the stable manifold of one Lissajous rev propagated backward in time. These trajectories are the ones that connect with the last resonance of the moon tour. In order to determine the value of the resonance associated to each trajectory, the manifold is propagated backwards in time until it crosses the negative x-axis, which is used as a Poincare section. Using the state at this intersection, the osculating semi-major axis with respect to Jupiter is used to determine the resonance at which each trajectory arrives.

A Lissajous orbit with parameters $A_y = 5500$ km and $A_z = 5500$ km is used to generate back-

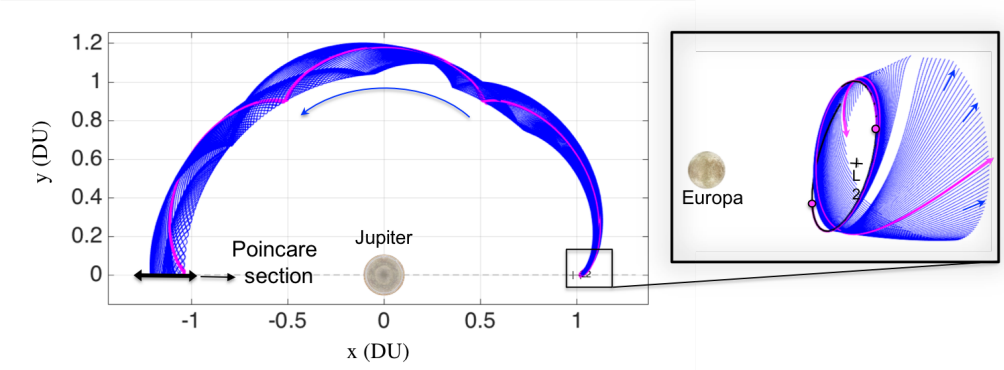

Figure 10. Backward propagation of the stable manifold of a Lissajous rev.

ward propagated manifolds to determine which resonance values are reachable, using a perturbation value of $\epsilon = 10^{-6}$. The Jacobi constant of this Lissajous is $J = 3.0031$. Figure 11 shows the manifolds in a semi-major axis versus τ (i.e., departure location from the Lissajous rev.) plot. The navy blue represents the solutions for the entire Lissajous ($0 \leq \phi \leq 360°$), whereas the cyan, magenta, and yellow correspond to specific Lissajous revs at $\phi = 0°$, $\phi = 45°$, and $\phi = 315°$, respectively. Four families emerge for the entire Lissajous orbit, each family corresponding to a quarter revolution of Lissajous revs. Figure 13 shows characteristics of the approximate invariant manifold of the same Lissajous orbit. Figure 13(a) is a plot of the out-of-plane component at the negative x-axis crossing versus the out-of-plane component at the departure from the Lissajous. Figure 13(b) shows the set of manifold trajectories in a semi-major axis versus the negative x-axis crossing value. The same oscillatory behavior as for the Lyapunov and halo families is observed. Figures 13(c) and (d) show the range of inclination and eccentricity coverage by the set of manifold solutions.

The departure location from the Lissajous rev, respresented as $0 \leq \tau \leq 1$, determines the resonance value reached by the manifold trajectory. For example, in Figure 11, at $\phi = 45°$ (magenta), a 5:6 resonant is reached by departing at $\tau = 0.70$, a 6:7 is reached at $\tau = 0.51$, and a 7:8 is reached at $\tau = 0.38$. However, for other Lissajous revs, such as $\phi = 0°$ (cyan), a 5:6 resonance cannot be reached for any value of τ. The trajectories that depart the Lissajous rev corresponding to $\phi = 45°$ at three different τ values are shown in Figure 12. The plot on the left is Jupiter centered, and the three resonant trajectories are depicted. The plot on the right is a zoomed in view, showing the departure locations from the Lissajous rev. It is worth noting that not all the revs belonging to the same Lissajous have the same reachable resonances. Therefore, the selection of the Lissajous rev for staging purposes has to be carefully selected in the design process.

A similar analysis is done for the entire Lissajous database, and the results are grouped by A_y. Recall that for each A_y value, the database is generated by sweeping A_z from 2000 km $\leq A_z \leq$ 12000 km by intervals of 100 km. Figure 14 shows the backward propagated manifolds in a semi-major axis versus τ plot. The smallest range of possible resonances reached corresponds to the Lissajous with smallest A_y. As A_y increases, so does the range of reachable resonant values. For example, for $A_y = 6500$ km, the resonances 8:9, 7:8, 6:7, and 5:6 can be reached. This result is due to the fact that as A_y increases, the Jacobi constant range increases too, covering lower Jacobi constants, i.e., higher energy levels (see Figure 15(a)). An interesting feature in Figure 14 is that the semi-major axis values are centered around the 6:7 resonance. In the Jupiter-Europa system,

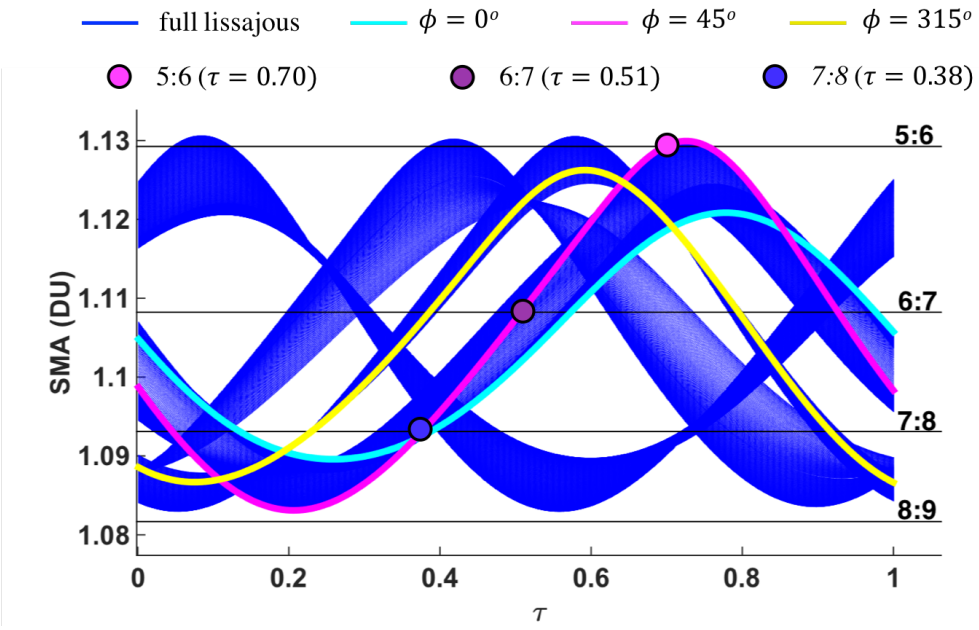

Figure 11. Semi-major axis at the negative x-axis crossing vs. departure location from the Lissajous, for a Lissajous orbit with $A_y = 5500$ km and $A_z = 5500$ km.

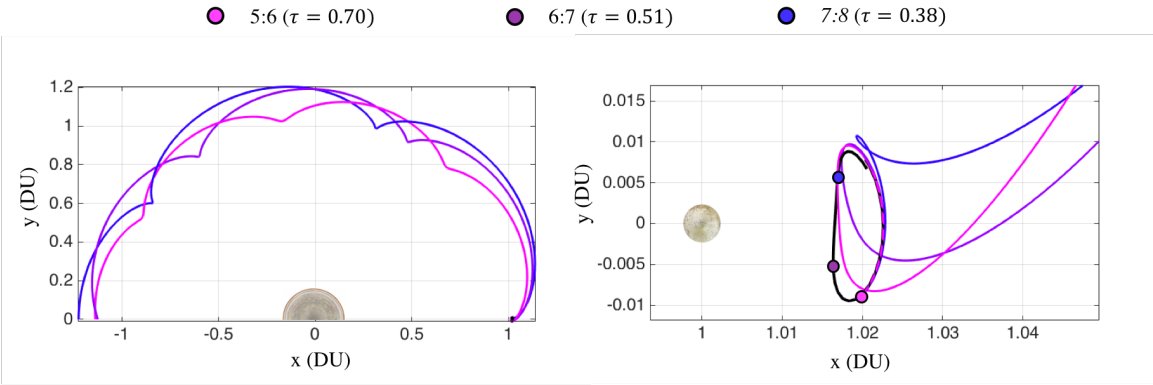

Figure 12. Backward propagated manifold from a Lissajous rev with parameters $A_y = 5500$ km, $A_z = 5500$, and $\phi = 45°$, from three different departing locations, reaching three different resonant trajectories.

the 6:7 resonance is the only one reachable at the lowest energy level at which free capture/escape trajectories are possible ($J \approx J_{L_2}$, where J_{L_2} is the Jacobi constant of a stationary point located at L_2[15]). As the energy increases, other resonant trajectories are reachable. For example, the 5:6 resonance is reachable for Jacobi constants below 3.0033 (Figure 15(a)) or for $A_y \geq 5500$ km (Figure 14).

Figure 15(b) shows the set of manifold trajectories from the Lissajous database in a semi-major axis versus negative x-axis crossing value. Opposite to Figure 15(a) where the data is spread in a cone-like area, in (b) all the points are condensed in an approximate line, which is due to purely geometrical reasons. The periapse for all manifold trajectories is approximately fixed at L_2. There-

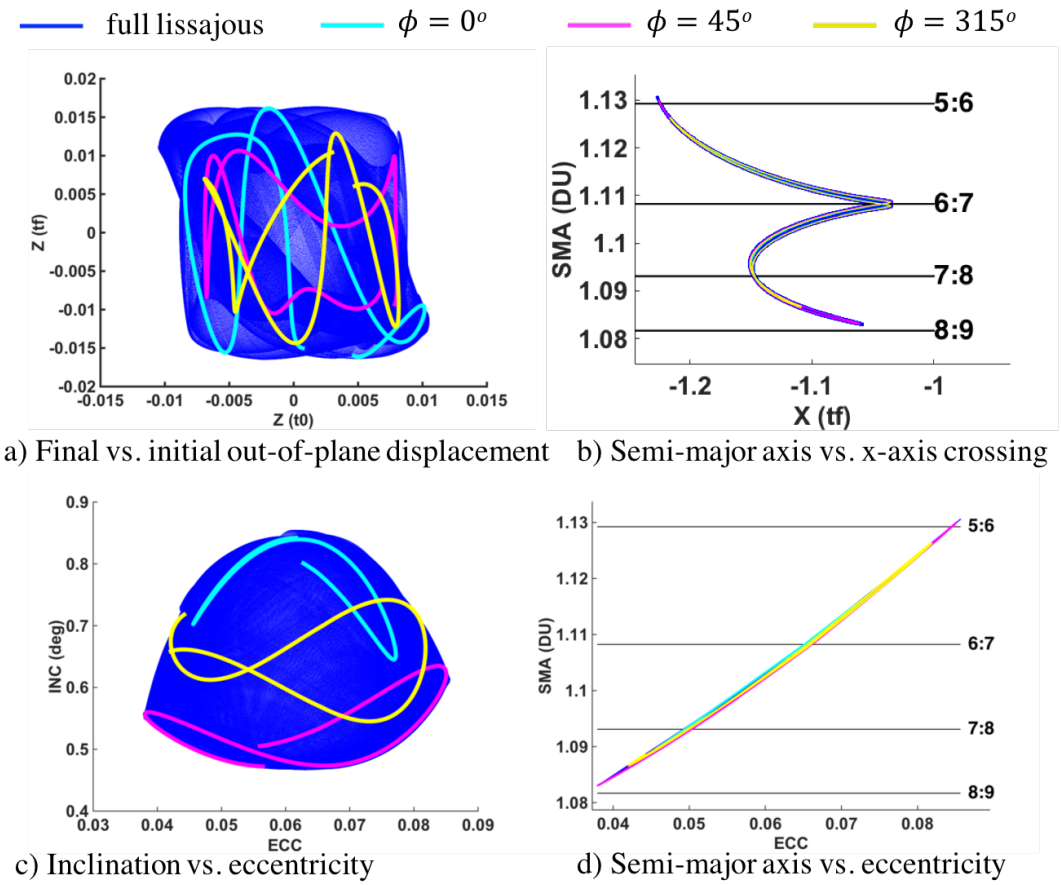

Figure 13. Orbit parameters for backward propagated manifold from a Lissajous orbit with $A_y = 4500$ km and $A_z = 4500$.

fore, for a fixed semi-major axis, the osculating apoapsis is approximately fixed, and hence, there is a one-to-one relationship between the x-axis crossing (in the rotating frame) and the semi-major axis. Figure 15(c) shows the range of inclination and eccentricity coverage by the set of manifold solutions. For higher amplitude A_y, the range of eccentricity and inclination is larger. The eccentricity is centered at 0.06. Two families become apparent when looking at the data in the semi-major axis versus eccentricity plot in Figure 15(d). The reason for this is unknown, and the authors are investigating the reasoning.

Timing and Phasing Control at Lissajous Arrival

In the previous examples, the manifolds were generated using a fixed perturbation $\epsilon = 1e-6$. Note that by fixing the value of ϵ, a degree of freedom is lost. However, variations in ϵ, corresponding to different departure times, are equivalent to solutions associated with different values of τ (see Reference 16). Therefore, ϵ can be used as a phasing control. Figure 16(a) shows in magenta the semi-major axis versus τ curve corresponding to the same manifold coming from the Lissajous rev shown in Figure 11, with $A_y = 5500$ km, $A_z = 5500$ km, and $\phi = 45°$. This curve was generated using $\epsilon = 1e-6$, which corresponds to a $\Delta v = 2 \cdot 10^{-4}$ m/s and $\Delta r = 150$ m. Manifold trajec-

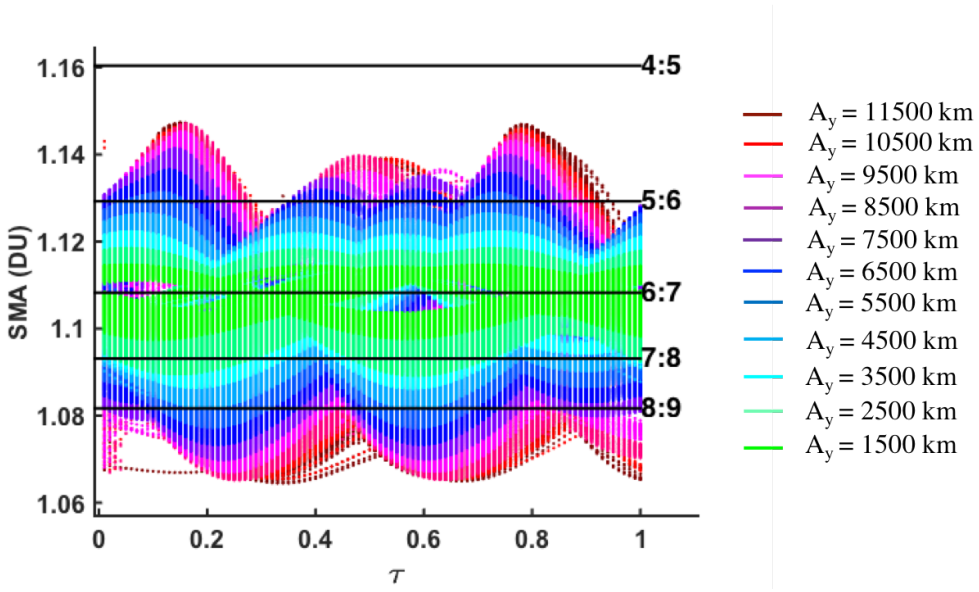

Figure 14. Semi-major axis at the negative x-axis crossing vs. departure location from the Lissajous, for the entire Lissajous database.

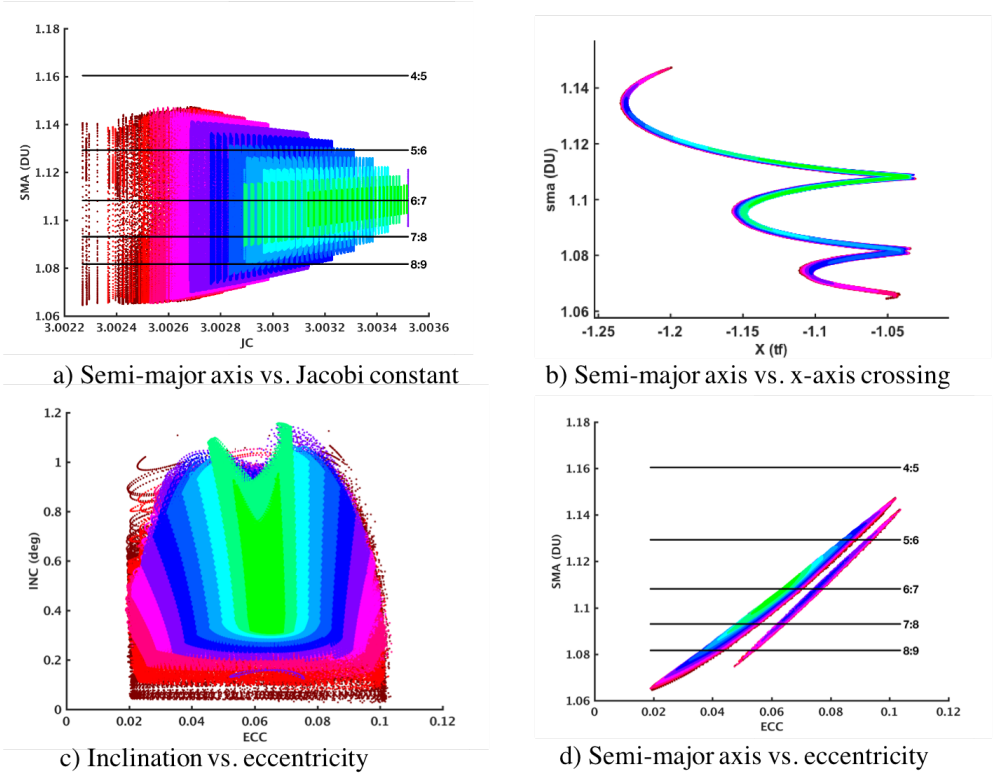

a) Semi-major axis vs. Jacobi constant

b) Semi-major axis vs. x-axis crossing

c) Inclination vs. eccentricity

d) Semi-major axis vs. eccentricity

Figure 15. Orbit parameters for backward propagated manifolds for the entire Lissajous database.

tories coming from the same Lissajous rev were generated using different values of ϵ. The effect of varying the perturbation size is shown in the same figure, which creates a shift in the phase of the

sinusoidal behavior of the curve. For example, the resonance 6:7 can be reached at $\tau \approx 0.5$ when using a perturbation $\epsilon = 1e-6$. To reach this same resonance but at $\tau \approx 0.25$, an $\epsilon = 4e-6$ can be used. Therefore, ϵ can be used as a parameter to control the time of arrival at the staging Lissajous orbit.

Figure 16(b) shows four different trajectories associated with $\tau = 0.38$ using the four perturbation sizes shown in the legend in Figure 16(a). The different arrival resonances are apparent. Although the perturbation magnitude is varying, it is still small enough that is does not change the Jacobi constant or energy of the trajectories (which is the same than that of its associated Lissajous). Note that changing the perturbation does not change the amplitude of the sinusoidal-like curves; only a shift in arrival/departure is achieved. Therefore, the resonances that can be reached from a given Lissajous rev orbit do not vary under changes on the perturbation. Recall the curve in Figure 11 associated to $\phi = 0°$ (cyan). From this Lissajous rev, only resonances 6:7 and 7:8 can be reached, no matter which values of τ or ϵ are used. Figure 16(c) shows four different manifold trajectories, leaving at different τ values, using the four perturbation sizes shown in the legend in Figure 16(a). All the trajectories here arrive at a 5:6 resonance, showing how it is possible to control the arrival phasing at the Lissajous orbit by varying the perturbation size.

CONCLUSION

This paper investigates libration point orbits at L_2 in the Jupiter-Europa system as staging orbits to connect to the last resonance of a moon tour. This strategy allows the decoupling of the moon tour phase with the capture/landing phase in order to satisfy multiple requirements. The strategy is based on the computation of invariant manifolds of libration point orbits, that, propagated backward in time, can be used as free capture connections with the moon tour.

The libration point orbits used are Lyapunov, halo, and Lissajous orbits. Lissajous orbits have been found to give more flexibility in the design and for phasing control. The computation of approximate invariant manifolds of the Lissajous torus is obtained by computing approximate invariant manifolds of individual Lissajous revs, allowing for a simple, systematic strategy. Multiple resonances can be reached from a single Lissajous orbit, and the range of resonances depends directly on the Lissajous dimension, i.e. in-plane and out-of-plane amplitude. By parametrizing the departure location from a Lissajous rev, a direct control over the specific desired resonance to be reached is possible. It was found that different revs belonging to a same Lissajous rev produce a different range of reachable resonances. A timing control on when to arrive at the Lissajous rev from a same resonant trajectory is possible by varying the perturbation size of the departing invariant manifold (which is propagated backward in time). This allows for freedom in staging at the Lissajous orbit, which is key in desiginign a landing trajectory at the desired location and local solar time.

ACKNOWLEDGMENT

The authors would like to thank Tim McElrath for his mentoring during this study. This research was carried out at the Jet Propulsion Laboratory, California Institute of Technology, under a contract with the National Aeronautics and Space Administration.

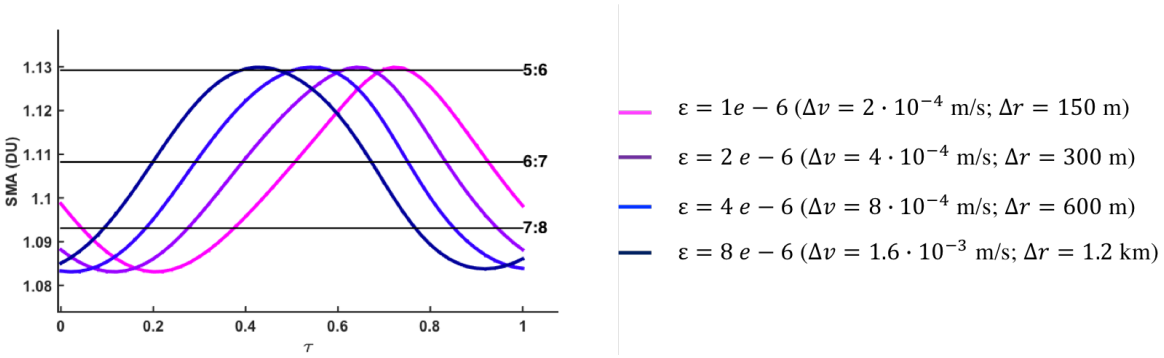

(a) Semi-major axis at the negative x-axis crossing vs. departure location from the Lissajous rev. Perturbation sizes and equivalent velocity and position displacement are noted in the legend.

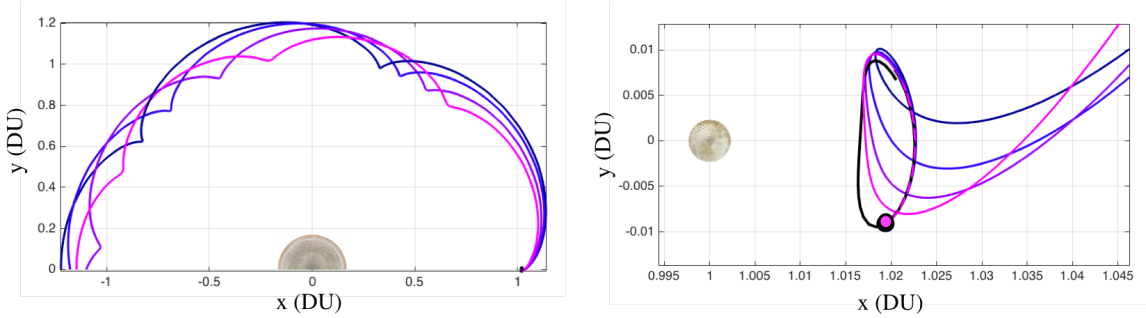

(b) Manifold trajectories reach different resonances when departing from the same $\tau = 0.38$ at different ϵ.

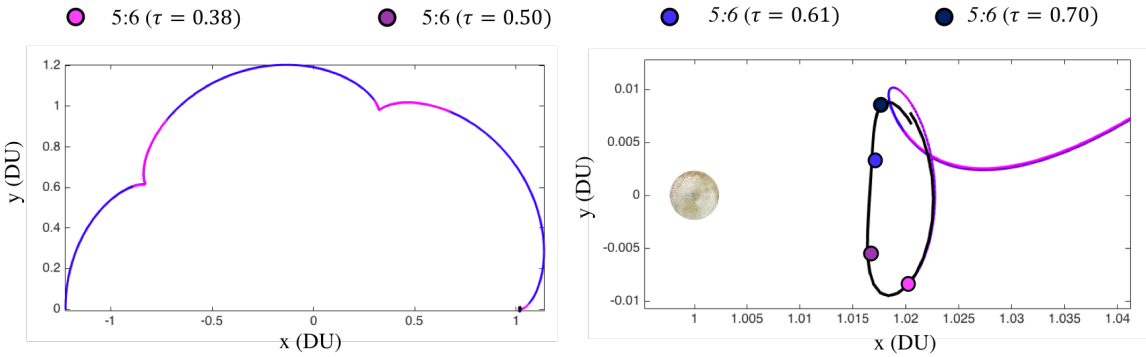

(c) Manifold trajectories reach the same 5:6 resoance when departing from different τ and propagated at different ϵ.

Figure 16. Backward propagated manifolds from a Lissajous rev with parameters $A_y = 5500$ km, $A_z = 5500$ km, $\phi = 45°$ with varying ϵ values.

REFERENCES

[1] R. L. Restrepo, R. P. Russell, and M. W. Lo, "Europa Lander Trajectory Design Using Lissajous Staging Orbits," AAS/AIAA *Astrodynamics Specialist Conf., AAS 18-491*, Snowbird, UT, Aug. 2018.

[2] R. L. Anderson and J. S. Parker, "Survey of Ballistic Transfers to the Lunar Surface," *Journal of Guidance, Control, and Dynamics*, Vol. 35, July - August 2012, pp. 1256–1267.

[3] R. L. Anderson and J. S. Parker, "Comparison of Low-Energy Lunar Transfer Trajectories to Invariant Manifolds," *Celestial Mechanics and Dynamical Astronomy*, Vol. 115, February 2013, pp. 311–331.

[4] J. S. Parker and R. L. Anderson, "Targeting Low-Energy Transfers to Low Lunar Orbit," *Acta Astronautica*, Vol. 84, March-April 2013, pp. 1–14.

[5] J. S. Parker, R. L. Anderson, and A. Peterson, "Surveying Ballistic Transfers to Low Lunar Orbit," *Journal of Guidance, Control, and Dynamics*, Vol. 36, No. 5, 2013, pp. 1501–1511.

[6] R. L. Anderson, "Approaching Moons from Resonance via Invariant Manifolds," *Journal of Guidance, Control, and Dynamics*, Vol. 38, June 2015, pp. 1097–1109.

[7] R. L. Anderson and M. W. Lo, "Spatial Approaches to Moons from Resonance Relative to Invariant Manifolds," *Acta Astronautica*, Vol. 105, 2014, pp. 355–372.

[8] R. L. Restrepo and R. P. Russell, "Catalog of Periodic Orbits for Planets and Main Planetary Satellites in the Solar System," AAS/AIAA *Astrodynamics Specialist Conference, No. AAS 17-964*, Stevenson, WA, August 2017.

[9] K. Howell, "Three-dimensional, periodic, 'halo' orbits," *Celestial Mechanics and Dynamical Astronomy*, Vol. 32, No. 1, 1984, pp. 53–71.

[10] R. P. Russell and T. Lam, "Designing Ephemeris Capture Trajectories at Europa Using Unstable Periodic Orbits," *Journal of Guidance, Control, and Dynamics*, Vol. 30, March-April 2007.

[11] G. Gómez, W. S. Koon, M. W. Lo, J. E. Marsden, J. J. Masdemont, and S. D. Ross, "Connecting orbits and invariant manifolds in the spatial restricted three-body problem," *Nonlinearity*, Vol. 17, September 2004, pp. 1571–1606.

[12] R. L. Anderson, "Approaching Moons from Resonance via Invariant Manifolds," *Journal of Guidance, Control, and Dynamics*, Vol. 38, No. 6, 2015, pp. 1097–1109, 10.2514/1.G000286.

[13] K. C. Howell and H. Pernicka, "Numerical Determination of Lissajous Trajectories in the Restricted Three-Body Problem," *Celestial Mech.*, Vol. 41, 1988, pp. 107–124.

[14] D. L. Richardson and N. D. Cary, "A Uniformly Valid Solution for Motion About the Interior Libration Point of the Perturbed Elliptic-Restricted Problem," *AAS/AIAA Astrodynamics Specialist Conference, Nassau, Bahamas, July 28-30*, 1975.

[15] R. L. Restrepo and R. P. Russell, "A Database of Planar Axisymmetric Periodic Orbits for the Solar System," *Celestial Mechanics and Dynamical Astronomy*, Vol. 130, July 2018, p. 49, 10.1007/s10569-018-9844-6.

[16] G. Lantoine and R. P. Russell, "Near Ballistic Halo-to-Halo Transfers between Planetary Moons," *The Journal of the Astronautical Sciences*, Vol. 58, No. 3, 2011, pp. 335–363.